Molecular Road Map to Tuning Ground State Absorption and Excited State Dynamics of Long-Wavelength Absorbers

Yusong Bai,[a] Jean-Hubert Olivier,[a] Hyejin Yoo,[a] Nicholas F. Polizzi,[a] Jaehong Park,[a,b] Jeff Rawson,[a] and Michael J. Therien[a*]

[a]Department of Chemistry, French Family Science Center, 124 Science Drive, Duke University, Durham, North Carolina 27708-0346, USA

[b]Department of Chemistry, University of Pennsylvania, 231 South 34th Street, Philadelphia, PA 19104-6323, USA

Abstract

Realizing chromophores that simultaneously possess substantial near-infrared (NIR) absorptivity and long-lived, high-yield triplet excited states is vital for many optoelectronic applications, such as optical power limiting and triplet-triplet annihilation photon upconversion (TTA-UC). However, the energy gap law ensures such chromophores are rare, and molecular engineering of absorbers having such properties has proven challenging. Here, we present a versatile methodology to tackle this design issue by exploiting the ethyne-bridged (polypyridyl)metal(II) (**M**; **M** = **Ru**, **Os**)-(porphinato)metal(II) (**PM'**; **M'** = **Zn**, **Pt**, **Pd**) molecular architecture (**M-(PM')$_n$-M**), wherein high-oscillator-strength NIR absorptivity up to 850 nm, near-unity intersystem crossing (ISC) quantum yields (Φ_{ISC}), and triplet excited-state (T_1) lifetimes on the μs timescale are simultaneously realized. By varying the extent to which the atomic coefficients of heavy metal d-orbitals contribute to the one-electron excitation configurations describing the initially prepared singlet and triplet excited-state wavefunctions, we: (i) show that the relative magnitudes of fluorescence (k_F^0), $S_1 \rightarrow S_0$ non-radiative decay (k_{nr}), $S_1 \rightarrow T_1$ ISC (k_{ISC}), and $T_1 \rightarrow S_0$ relaxation ($k_{T1 \rightarrow S0}$) rate constants can be finely tuned in **M-(PM')$_n$-M** compounds, and (ii) demonstrate designs in which the k_{ISC} magnitude dominates singlet manifold relaxation dynamics, but does not give rise to $T_1 \rightarrow S_0$ conversion dynamics that short-circuit a μs timescale triplet lifetime. Notably, the NIR spectral domain absorptivities of **M-(PM')$_n$-M** chromophores far exceed those of classic coordination complexes and organic materials possessing similarly high yields of triplet-state formation: in contrast to these benchmark materials, this work demonstrates that these **M-(PM')$_n$-M** systems realize near unit Φ_{ISC} at extraordinarily modest S_1-T_1 energy gaps (~0.25 eV). This study underscores the photophysical diversity of the **M-(PM')$_n$-M** platform, and presents a new library of long-wavelength absorbers that efficiently populate long-lived T_1 states.

Introduction

Strong near-infrared (NIR) absorbing chromophores featuring long-lived triplet excited states produced at near-unit quantum yield are key to various optoelectronic applications that include long-wavelength optical power limiting (OPL),[1] dye-sensitized solar cell (DSSC), [2] and emerging photon-upconversion (UC) technologies, [3] such as those based on the triplet-triplet annihilation (TTA) mechanism. However, engineering such NIR chromophores remains extremely challenging, as diminishing the optical bandgap of a given molecular absorber exponentially increases its nonradiative ($S_1 \rightarrow S_0$) transition rate constant congruent with the energy gap law, [4] which serves to dramatically reduce the corresponding $S_1 \rightarrow T_1$ intersystem crossing (ISC) quantum yield. [4-5]

Over the past several decades, long-lived triplet excited states formed at unitary conversion have been predominantly realized in (polypyridyl)metal complexes, wherein $S_1 \rightarrow T_1$ ISC gives rise to metal-to-ligand charge transfer triplet (^{3}MLCT) states.[6] However, metal complexes of this genre suffer from weak long-wavelength absorptivity relative to those evinced by many organic dyes. [7] In this regard, porphyrin-based pigments have been widely explored for crafting NIR chromophores. [8] While high oscillator strength ($\varepsilon > 10^5$ $M^{-1}cm^{-1}$), broad NIR (>700 nm) absorptivity has been achieved in selected classes of these porphyrin-based compositions, [9] the majority of these constructs feature fast excited-state relaxation within the singlet manifolds, resulting in ISC dynamics that give rise to low triplet state yields.[9h,10] Within this context, engineering strong NIR-absorbing chromophores having long-lived T_1 excited states and fast $S_1 \rightarrow T_1$ relaxation dynamics has remained a formidable challenge.

Here, we describe a molecular design road map to access chromophores that not only feature high oscillator strength NIR-absorptive manifolds that span the 700-900 nm spectral domain, but also manifest near-unity population of long-lived triplet excited states following photoexcitation. This design strategy exploits the symmetric molecular architecture of highly-absorptive ethyne-bridged (polypyridyl)metal(II) (**M**; **M** = **Ru**, **Os**) -(porphinato)metal(II) (**PM'**; **M'** = **Zn**, **Pt**, **Pd**) compounds (**M-(PM')$_n$-M**), wherein the nature of the chromophore-to-chromophore connectivity drives substantial mixing of porphyrin-based π-π* and metal polypyridyl-based charge-resonance transitions. We analyze the influences of **PM'** conjugation length and the nature of the metal ion upon $S_0 \rightarrow S_1$ and $S_0 \rightarrow T_1$ energy gaps, and the $S_1 \rightarrow T_1$ ISC and $T_1 \rightarrow S_0$ relaxation rate constant magnitudes. Spectroscopic data underscore that conjugation extension along the long molecular axis achieved through **PM'** conjugation: i) dramatically redshifts the $S_0 \rightarrow S_1$ absorption band and enhances its NIR transition oscillator strength; ii) has a relatively modest influence on the S_0-T_1 energy gap; and iii) reduces the (terpyridyl)metal d-orbital contribution to the

initially prepared **M-(PM')$_n$-M** S_1 state wavefunction and hence decreases the magnitude of the ISC rate constants in the corresponding **M-(PM')$_n$-M** chromophores. These data further demonstrate that this third effect derives from the increasing contribution of porphyrin-based π-π* character to the $S_0 \rightarrow S_1$ transition with increasing conjugation. In this regard, divalent Pt and Pd ions within the **(PM')$_n$** chromophoric fragments of these **M-(PM')$_n$-M** supermolecules can be exploited as tools to tune the extent to which heavy metal d-orbitals contribute to the one-electron excitation configurations that describe the initially prepared singlet excited state. As such, not only high oscillator strength NIR absorptivities are made possible: because the relative magnitudes of fluorescence (k_F^0), $S_1 \rightarrow S_0$ non-radiative decay (k_{nr}), $S_1 \rightarrow T_1$ ISC (k_{ISC}), and $T_1 \rightarrow S_0$ relaxation ($k_{T1 \rightarrow S0}$) rate constants can be finely tuned in **M-(PM')$_n$-M** compounds, exceptional T_1-state quantum yields can be realized in these structures. Given these enhanced photophysical properties, **M-(PM')$_n$-M** chromophores stand in sharp contrast to extensive families of conventional metal complexes, organic molecules, and polymer materials such as (polypyridyl)metal(II) complexes, [11] bodipy derivatives, [3b] and polythiophene derivatives [12] that have been traditionally utilized for OPL, TTA-UC, and DSSC applications.

Experimental Section

1. Synthesis and Characterization. A full account of the synthesis and characterization of all new compounds, complete with detailed reaction schemes, is provided in the Supporting Information.

2. Instrumentation. Electronic absorption spectra were recorded on a Shimadzu UV-1700 spectrophotometer, and emission spectra were recorded on an Edinburgh Instruments FLS920 luminescence spectrometer that utilized a T-channel configuration and PMT/InGaAs/Extended-InGaAs detectors. Emission spectra were corrected using the spectral output of a calibrated light source supplied by the National Bureau of Standards. Low temperature (77 K) spectra were recorded using an optical Dewar. Luminescent lifetimes were determined by a streakscope-based Hamamatsu picosecond fluorescence lifetime measurement system (see below).

3. Picosecond Fluorescence Lifetime Measurement System (Streakscope). Time-resolved emission spectra were recorded using a Hamamatsu C4780 picosecond fluorescence lifetime measurement system. This system employs a Hamamatsu Streakscope C4334 as its photon-counting detector; a Hamamatsu C4792-01 synchronous delay generator electronically generated all time delays. A Hamamatsu 405 nm diode laser was utilized as the excitation source. All fluorescence data were acquired in single-photon-counting mode using Hamamatsu HPD-TA software. The data were analyzed using the Hamamatsu fitting module; both non-deconvoluted and

deconvoluted data analyses were performed to ascertain whether or not any emissive processes were excitation pulse-limited.

4. **Femtosecond and Nanosecond Transient Absorption Experiments.** The transient optical system utilized in this work has been discussed previously. [13] All the samples for pump-probe experiments were deoxygenated via three successive freeze-pump-thaw cycles prior to measurement.

Results and Discussion

Scheme 1. Syntheses and chemical structures of **M-(PM')** $_n$**-M** chromophores

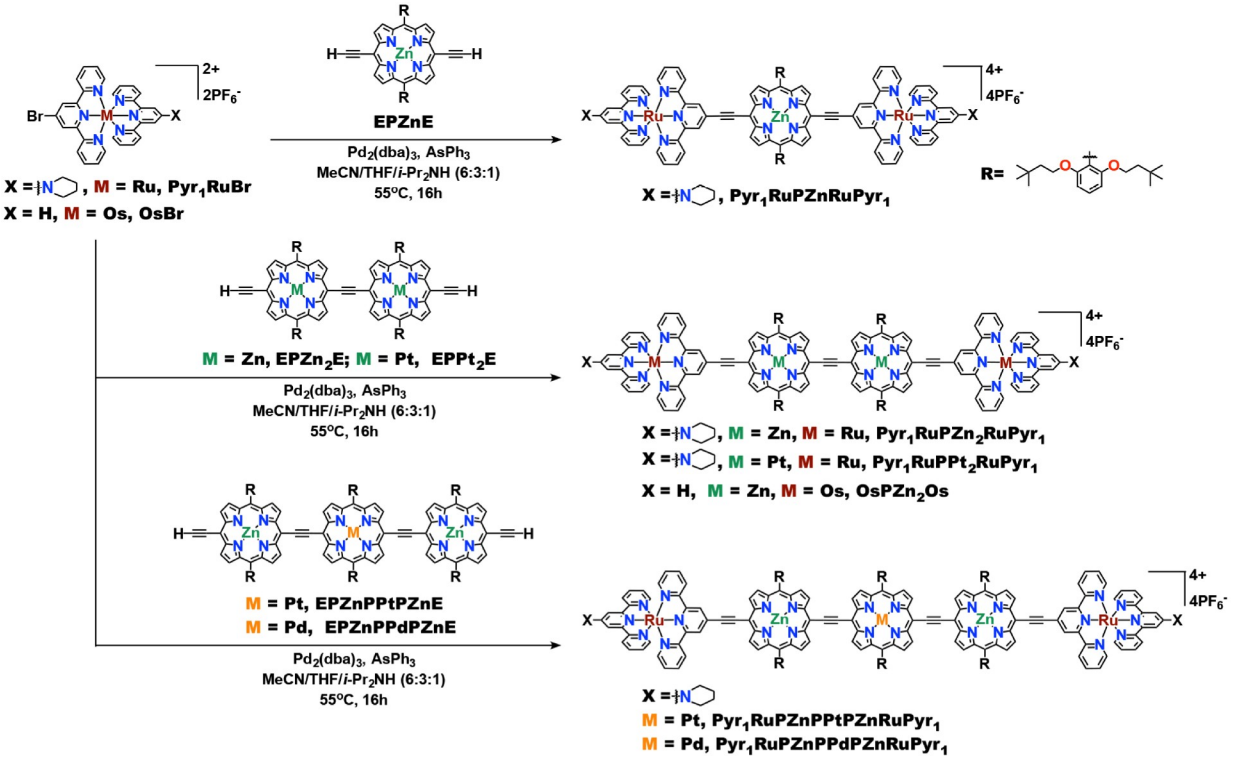

1. Synthesis. Scheme 1 summarizes the strategies employed in the syntheses of ethyne-bridged oligo(porphinato)metal(II)-bis(terpyridyl)metal(II) chromophores **Pyr** $_1$**RuPZnRuPyr**$_1$, **Pyr**$_1$**RuPZn**$_2$**RuPyr**$_1$, **OsPZn**$_2$**Os**, **Pyr**$_1$**RuPPt**$_2$**RuPyr**$_1$, **Pyr**$_1$**RuPZnPPtPZnRuPyr** $_1$, and **Pyr**$_1$**RuPZnPPdPZnRuPyr** $_1$. Detailed synthetic procedures for these chromophores can be found in the Supporting Information. Ruthenium(II) (4'-bromo-2,2';6',2''-terpyridine)(4'-pyrrolidin-1-yl-2, 2,2';6',2''-terpyridine) bis(hexafluorophosphate) (**Pyr** $_1$**RuBr**), osmium(II) (4'-bromo-2,2';6',2''-terpyridine)(2, 2,2';6',2''-terpyridine) bis(hexafluorophosphate) (**OsBr**) and [5,15-bis-ethynyl-10,20-di(2',6'-bis(3,3-dimethyl-1-butyloxy)phenyl)porphinato]zinc(II) (**EPZnE**) were synthesized according to published procedures. [14] The syntheses of bis-ethynyl-oligo(porphinato)metal(II) precursor complexes

(**EPZn$_2$E**, **EPPt$_2$E**, **EPZnPPtPZnE**, **EPZnPPdPZnE**) are discussed in the Supporting Information. In general, the supermolecular chromophores were prepared through metal-mediated cross-coupling [15] of a *meso*-ethyne-functionalized (porphinato)metal(II) species with 4'-brominated bis(2, 2,2';6',2''-terpyridyl)metal(II) compounds (**Scheme 1**; Supporting Information). Details concerning reaction conditions, reaction yields, and purification procedures for the Scheme 1 supermolecular chromophores may be found in the Supporting Information.

2. Steady-State Electronic Absorption Spectroscopy. As shown in **Figure 1**, **M-(PM')$_n$-M** display an unusual degree of spectral coverage over the visible (vis) and NIR regime, tailing to 900 nm. Such high oscillator strength vis-to-NIR absorptivities derive largely from the porphyrinic components and the nature of chromophore-to-chromophore connectivity in these systems: the ethyne-linkage topology aligns the chromophoric transition dipoles along the long molecular axis (x-axis) and promotes effective mixing between the porphyrin π-π* and metal polypyridyl-based charge-resonance transitions, resulting in redistribution of the oscillator strength spanning vis-to-NIR spectral domain. [9a,9b,14b,14c,15d,16] In this regard, several characteristic electronic transitions are highlighted: (i) a broad, high-oscillator-strength absorption manifold ($\varepsilon > 100{,}000\ M^{-1}\ cm^{-1}$) that spans the 400-500 nm spectral window which manifests significant porphyrin-derived ^{1}π-π* Soret (B) band transition, [9a,9b,14b,14c] (ii) the red-edge of the B-band absorption (500-550 nm) that features $[Ru(tpy)_2]^{2+}$-derived ^{1}MLCT transition character, [14b,14c] and (iii) the absorption band in the long-wavelength (> 600 nm) domain of the spectrum which exhibits porphyrinic ^{1}π-π* Q-state character (**Table 1**). [9a,9b,14b,14c,16] We note that although the "B", "Q", and "MLCT" labels are preserved throughout this report for describing characteristic **M-(PM')$_n$-M** electronic absorption manifolds, they suggest only the dominant characters of these transitions, as the B, Q, and MLCT electronic states mix extensively in **M-(PM')$_n$-M** chromophores.

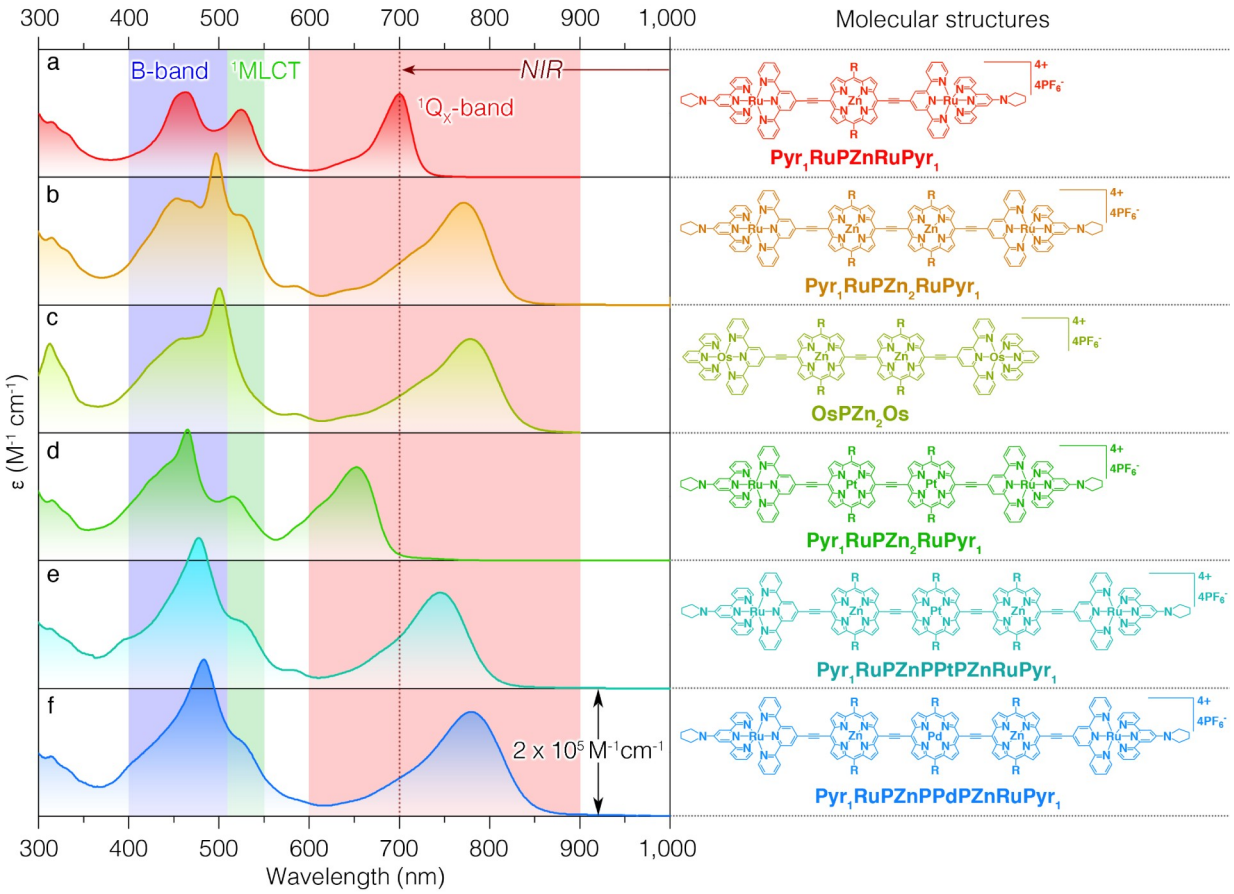

Figure 1. Steady-state electronic absorption spectra of: (a) **Pyr $_1$RuPZnRuPyr$_1$**, (b) **Pyr$_1$RuPZn$_2$RuPyr$_1$**, (c) **OsPZn$_2$Os**, (d) **Pyr$_1$RuPPt$_2$RuPyr$_1$**, (e) **Pyr$_1$RuPZnPPtPZnRuPyr$_1$**, and (f) **Pyr$_1$RuPZnPPdPZnRuPyr$_1$**. Experimental conditions: solvent = acetonitrile, ambient temperature. The R group denotes 2'6'-bis(3,3-dimethyl-1butyloxy)phenyl.

As highlighted in **Figure 1**, NIR spectral domain absorptive characteristics are modulated through both conjugation length and the nature of the porphyrin central metal ion. Due to a combination of symmetry breaking effects that derive from extensive x-axis conjugation and charge-transfer character stems from the ethyne linkage motif that connects the (porphinato)metal(II) and (polypyridyl)metal(II) moieties, the **M-(PZn)$_n$-M** x-polarized Q-state transition (Q_x) manifold manifests a progressive redshift and oscillator-strength enhancement with elongation of porphyrinic conjugation,[9a,9b,14b,15a] highlighted in part by the **Pyr$_1$RuPZnRuPyr$_1$** and **Pyr$_1$RuPZn$_2$RuPyr$_1$** spectra (**Figure 1a-b**). Note also that the energy of Q_x absorption maximum is highly sensitive to porphyrin central metal ion selection: replacing zinc(II) with palladium(II) or platinum(II) results in hypsochromic shifts due to the mixing of porphyrin π* and metal ndπ orbitals (e.g., **Figure 1b, d**).[17] In this regard, **M-(PZn)$_n$-M** chromophores that exploit a component (porphinato)palladium(II) moiety display a less significant hypsochromic shift of the Q_x absorption

maximum relative to the analogous **M-(PZn)$_n$-M** chromophores that leverage (porphinato)platinum(II) unit (**Figure 1e-f**).[18]

Table 1. Ground State Electronic Absorption Spectral Data, Q_x-Manifold Integrated Oscillator Strengths, and NIR Spectral Coverage (FWHM) for **M-(PM')$_n$-M** Chromophores.[a]

Chromophores	EAS Band Maximum / nm (ε / 10^5 $M^{-1}.cm^{-1}$)			FWHM[b] / cm^{-1} Q_x-band	Oscillator Strength In NIR Regime[c]
	B-band Region	^{1}MLCT	Q-band Region		
$Pyr_1RuPZnRuPyr_1$	463 (1.33)	525 (1.06)	702 (1.30)	820	0.25
$Pyr_1RuPZn_2RuPyr_1$	453 (1.67), 464 (1.63) 497 (2.38)	522 (1.41)	583 (0.30) 772 (1.60)	1500	0.99
$OsPZn_2Os$	460 (1.48), 500 (2.26)	518 (1.22)	584 (0.30) 776 (1.47)	1630	0.96
$Pyr_1RuPPt_2RuPyr_1$	465 (2.05)	515 (1.00)	653 (1.46)	1800	0.02
$Pyr_1RuPZnPPtPZnRuPyr_1$	477 (2.36)	523 (1.05)	582 (0.29) 746 (1.50)	1550	0.85
$Pyr_1RuPZnPPdPZnRuPyr_1$	483 (2.45)	524 (1.19)	584 (0.27) 780 (1.63)	1700	1.13

[a] From electronic absorption spectra recorded in acetonitrile solvent. [b] Taken as the spectral width of the Q-band region at half the height of the lower-energy absorption noted. [c] Integrated oscillator strengths (f) were calculated based on the following expression: $f = 4.3 \times 10^{-9} \int \varepsilon \, dv$, where ε is the experimental extinction coefficient, and ν is the energy (in wave numbers) of the absorption. Oscillator strengths were calculated over the following wavelength domains: **$Pyr_1RuPZnRuPyr_1$** (700 - 800 nm); **$Pyr_1RuPZn_2RuPyr_1$** (700 - 900 nm); **$OsPZn_2Os$** (700 - 900 nm); **$Pyr_1RuPPt_2RuPyr_1$** (700 - 800 nm); **$Pyr_1RuPZnPPtPZnRuPyr_1$** (700- 900 nm); and **$Pyr_1RuPZnPPdPZnRuPyr_1$** (700 - 1000 nm).

Among these **M-(PZn)$_n$-M** chromophores, **$Pyr_1RuPZnPPdPZnRuPyr_1$** is an exceptional NIR absorber with a broad Q_x-derived manifold centered at 780 nm, having a full width at half-maximum (FWHM) of ~1700 cm^{-1}, and a substantial extinction coefficient (163,000 M^{-1} cm^{-1}). Note that, even at 850 nm, the absorptive extinction coefficients of **$Pyr_1RuPZnPPdPZnRuPyr_1$** still exceeds 15,000 $M^{-1}cm^{-1}$. These **$Pyr_1RuPZnPPdPZnRuPyr_1$** NIR absorptive characteristics surpass those of widely exploited long-wavelength absorbers that include conventional (polypyridyl)metal(II) derivatives,[11] bodipy chromophores,[3b] and polythiophene-based materials.[12]

3. Steady-State Emission Spectroscopy. The emission spectroscopy of all these **M-(PM')$_n$-M** chromophores were investigated to determine the energy levels of their respective S_1 and T_1 states (from respective $S_1 \rightarrow S_0$ fluorescence and $T_1 \rightarrow S_0$ phosphorescence data), and qualitatively map $S_1 \rightarrow T_1$ ISC efficiencies. **M-(PM')$_n$-M** emission spectra were measured at ambient temperature under both oxygenated and deoxygenated conditions (Supporting Information) in acetonitrile solvent. Under oxygenated conditions, $O_2(^1\Delta)$ emission is observed at ~1270 nm from all the **M-(PM')$_n$-M** solution samples, suggesting the production of a low-lying ^{3}[**M-(PM')$_n$-M**]* state. Note, however, that the intrinsic emissive properties of these **M-(PM')$_n$-M** chromophores are relatively complex: **$Pyr_1RuPZnRuPyr_1$**,

OsRuPZn$_2$Os, **Pyr$_1$RuPPt$_2$RuPyr$_1$**, and **Pyr$_1$RuPZnPPtPZnRuPyr$_1$** manifest room-temperature phosphorescence under deoxygenated conditions, while phosphorescence for **Pyr$_1$RuPZn$_2$RuPyr$_1$** and **Pyr$_1$RuPZnPPdPZnRuPyr$_1$** is only evinced under low-temperature (77K) conditions (**Figures S17-18**); moreover, fluorescence signals were observed in almost all of the **M-(PM')$_n$-M** compounds at ambient temperature under both deoxygenated and oxygenated conditions, except for **Pyr$_1$RuPPt$_2$RuPyr$_1$**, which exhibits only phosphorescence.

Table 2. Emission Energies and Quantum Yields for **M-(PM')$_n$-M** Chromophores.

Chromophores	Emission Energy[a] / eV		Φ_{Em}[c] / %	
	$S_1 \rightarrow S_0$	$T_1 \rightarrow S_0$	$S_1 \rightarrow S_0$	$T_1 \rightarrow S_0$
Pyr$_1$RuPZnRuPyr$_1$	1.67	1.25	0.04	0.02
Pyr$_1$RuPZn$_2$RuPyr$_1$	1.53	1.27	2.00	< 0.01[d]
OsPZn$_2$Os	1.52	1.17	0.10	< 0.01[d]
Pyr$_1$RuPPt$_2$RuPyr$_1$	N/A[b]	1.45	N/A[b]	0.92
Pyr$_1$RuPZnPPtPZnRuPyr$_1$	1.58	1.24	0.13	< 0.01[d]
Pyr$_1$RuPZnPPdPZnRuPyr$_1$	1.53	1.26	1.23	< 0.01[d]

[a] Values reported correspond to the energy of the maximal emission wavelength (λ_{em}(max)). [b] Denotes no fluorescence observed [c] Emission quantum yields were determined relative to the meso-to-meso ethyne-bridged bis[(porphinato)zinc(II)] chromophore (**PZn$_2$**) in THF solvent (Φ_F = 0.16).[10h] [d] Denotes a phosphorescence quantum yield too small to be accurately determined; only an upper limit is indicated.

Because fluorescence observed in **M-(PM')$_n$-M** chromophores originates from a ^1Q_x state-dominated relaxation to the ground state that directly competes with the $S_1 \rightarrow T_1$ ISC process, comparing the relative fluorescence intensities amongst these **M-(PM')$_n$-M** chromophores provides a qualitative measure of their $S_1 \rightarrow T_1$ ISC efficiencies (Φ_{ISC}). These data indicate Φ_F (**Pyr$_1$RuPPt$_2$RuPyr$_1$**) < Φ_F (**Pyr$_1$RuPZnRuPyr$_1$**) ≈ Φ_F (**OsPZn$_2$Os**) ≈ Φ_F (**Pyr$_1$RuPZnPPtPZnRuPyr$_1$**) < Φ_F (**Pyr$_1$RuPZnPPdPZnRuPyr$_1$**) < Φ_F (**Pyr$_1$RuPZn$_2$RuPyr$_1$**) (**Figure S16**). Notably, relative to **Pyr$_1$RuPZnRuPyr$_1$**, **Pyr$_1$RuPZn$_2$RuPyr$_1$** exhibits a Φ_F enhancement of a factor of 5 [Φ_F(**Pyr$_1$RuPZnRuPyr$_1$**) = 0.04 %, Φ_F(**Pyr$_1$RuPZn$_2$RuPyr$_1$**) = 2.0 %, see **Table 2** and **Figure S16**], underscoring that in **M-(PM')$_n$-M** systems, long-wavelength absorptive oscillator strength enhancement based on simple conjugation expansion through additional porphyrin units [**(PM')$_n$**] drives diminished Φ_{ISC}. **OsPZn$_2$Os** and **Pyr$_1$RuPPt$_2$RuPyr$_1$**, which feature conjugated frameworks essentially identical in size to that of **Pyr$_1$RuPZn$_2$RuPyr$_1$**, manifest enhanced Φ_{ISC} values as a result of the more substantial spin-orbit coupling induced by the respective replacement of osmium (for ruthenium) and platinum (for zinc). These data indicate that a diminished Φ_{ISC} driven by (**PM')$_n$** conjugation expansion can be effectively suppressed by selective **Pt** or **Pd** metallation of porphyrin macrocycle (**Figure 1A-D**).

For instance, compared to **Pyr$_1$RuPZn$_2$RuPyr$_1$**, **Pyr$_1$RuPZnPPtPZnRuPyr$_1$** and **Pyr$_1$RuPZnPPdPZnRuPyr$_1$** feature significantly enhanced Φ_{ISC} values, as qualitatively suggested by their relative Φ_F magnitudes. The markedly different steady-state emission spectra observed in various **M-(PM')$_n$-M** supermolecular structures trace their genesis to the disparate excited-state relaxation dynamics characteristic of these chromophores (*vide infra*).

4. Pump-Probe Transient Absorption Spectroscopy. We discuss the common features of pump-probe transient absorption spectra recorded for **M-(PM')$_n$-M** chromophores following $S_0 \rightarrow S_1$ photoexcitation, and quantitatively analyze their respective excited-state dynamics relying on the time-dependent evolution of the transient absorptive signatures characteristic of their singlet and triplet excited-state manifolds. The femtosecond-to-nanosecond timescale transient spectra recorded at selected time delays for **M-(PM')$_n$-M** chromophores are displayed in **Figures 2**-**4**. The early time-delay ($t_{delay} \sim 0.3$ ps) transient spectra of these **M-(PM')$_n$-M** chromophores share several common features: (i) bleaching signals in the B and Q_x-band regions, (ii) weak transient absorptions between the two dominant ground-state absorption bleaching signatures, and (iii) intense NIR transient absorption manifolds that feature extraordinary spectral breadth. Moreover, these **M-(PM')$_n$-M** chromophores manifest qualitatively similar time-dependent transient spectral evolution in the NIR regime: the decay of the initially-prepared NIR transient absorption signal ($S_1 \rightarrow S_n$) correlates with the rise of a new lower-energy NIR transient absorption band, suggesting the evolution of a new electronically excited state. These electronically excited states persist beyond the delay limit of the femtosecond pump-probe instrument. Nanosecond-to-millisecond pump-probe transient absorption measurements determine that the lifetimes of these long-lived **M-(PM')$_n$-M** excited states are confined to the μs timescale under deoxygenated conditions; the lifetimes of these states are diminished to a few hundred ns when these **M-(PM')$_n$-M** solutions are oxygenated (Supporting Information), indicating the triplet nature of these states. As such, the lower-energy NIR transient manifold corresponds to $T_1 \rightarrow T_n$ transitions (as highlighted in **Figures 2**-**4**), whose rise and decay quantitatively respectively characterize the $S_1 \rightarrow T_1$ ISC dynamics and T_1 state lifetimes of these **M-(PM')$_n$-M** chromophores.

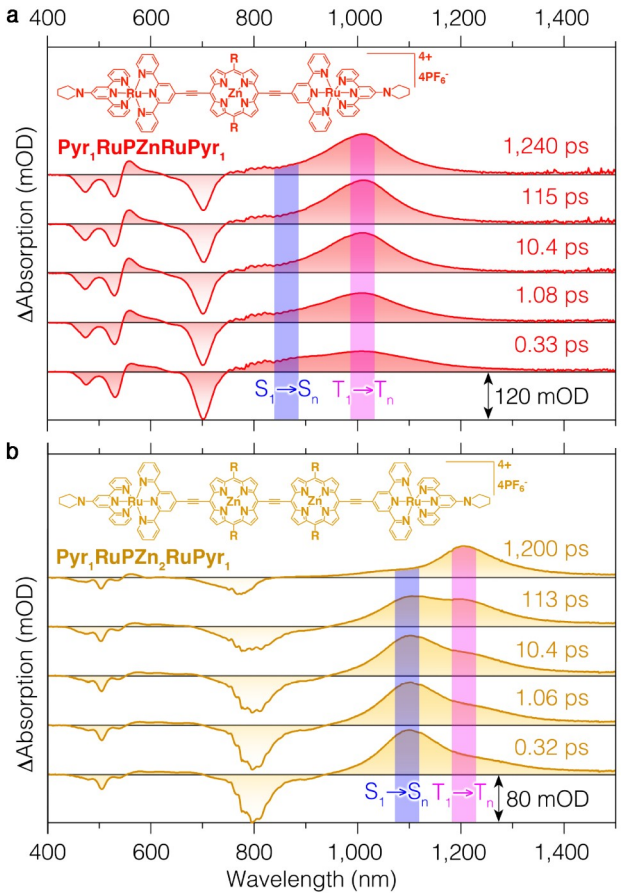

Figure 2. Transient absorption spectra determined at different time delays for (a) **Pyr $_1$RuPZnRuPyr$_1$** (λ_{ex} = 680 nm), and (b) **Pyr$_1$RuPZn$_2$RuPyr$_1$** (λ_{ex} = 800 nm). Experimental conditions: ambient temperature, pump power = 300 μW, solvent = acetonitrile, magic angle polarization.

A. Pyr$_1$RuPZnRuPyr$_1$ and Pyr$_1$RuPZn$_2$RuPyr$_1$. **Pyr$_1$RuPZnPyr$_1$** exhibits an ultrafast ISC rate constant and near-unit Φ_{ISC}. Φ_{ISC} can be calculated via the relation $\Phi_{ISC} = k_{ISC} / (k_{ISC} + k^0_F + k_{nr})$, wherein k_{ISC}, k^0_F, and k_{nr} are the respective rate constants for $S_1 \rightarrow T_1$ ISC, intrinsic $S_1 \rightarrow S_0$ fluorescence decay, and $S_1 \rightarrow S_0$ internal conversion processes. Since $\tau_{S1} = 1 / (k_{ISC} + k^0_F + k_{nr})$ and $\tau_{ISC} = 1 / k_{ISC}$, where τ_{S1} and τ_{ISC} correspond respectively to the S_1 state lifetime and the $S_1 \rightarrow T_1$ ISC time constant, Φ_{ISC} can be expressed as $\Phi_{ISC} = \tau_{S1} / \tau_{ISC}$.[5a] As discussed above, the $T_1 \rightarrow T_n$ transition manifold rise time quantitatively characterizes τ_{ISC}, while the decay time of the $S_1 \rightarrow S_n$ transition manifold provides a direct measure for τ_{S1}. In this regard, a global fit of the time-dependent NIR (800-1200 nm) transient absorption dynamics for **Pyr $_1$RuPZnPyr$_1$** enables determination of its intrinsic S_1 state lifetime and the $S_1 \rightarrow T_1$ ISC time constant: $\tau_{S1} \approx \tau_{ISC}$ ~0.80 ps (**Figure S28**). The evaluated magnitudes of τ_{S1} and τ_{ISC} enable the ^{1}[**M-(PM')$_n$-M**]* $\rightarrow$ ^{3}[**M-(PM')$_n$-M**]* ISC quantum yields to be determined; for **Pyr $_1$RuPZnPyr$_1$**, note that Φ_{ISC} is ~1.

Compared to **Pyr$_1$RuPZnRuPyr$_1$**, **Pyr$_1$RuPZn$_2$RuPyr$_1$** displays a dramatically diminished $S_1 \rightarrow T_1$ k_{ISC}, and a significantly suppressed Φ_{ISC}. Note that within the NIR spectral domain, **Pyr $_1$RuPZnRuPyr$_1$** manifests a $T_1 \rightarrow T_n$

transient absorption signal at the earliest time delays (t_{delay} ~300 fs), whereas electronically excited **$Pyr_1RuPZn_2RuPyr_1$** features a NIR transient absorption dominated by a $S_1 \rightarrow S_n$ transition over t_{delays} that range from 0.3-120 ps (**Figure 2**); these **$Pyr_1RuPZn_2RuPyr_1$** transient spectra acquired over these time delays resemble those evinced for the *meso*-to-*meso* ethyne-bridged bis[(porphinato)zinc] chromophore, **PZn_2**.[10c,10h] Congruent with these marked differences observed in the transient spectra, **$Pyr_1RuPZn_2RuPyr_1$** demonstrates dramatically different excited state relaxation dynamics relative to **$Pyr_1RuPZnRuPyr_1$**. A global fit of the time-dependent $S_1 \rightarrow S_n$ transient absorption dynamical data evinces three time components: 970 ± 130 fs, 60 ± 7 ps, 340 ± 20 ps; these are associated respectively with acetonitrile solvent relaxation, conformational relaxation, and the intrinsic singlet lifetime of **$Pyr_1RuPZn_2RuPyr_1$**. An analogous global fit of the $T_1 \rightarrow T_n$ transient dynamical data provides similar characteristic time components for solvent relaxation and conformational relaxation dynamics ($\tau_{solvent}$ ~800 fs; $\tau_{conformational}$ ~58 ps), whereas the third time component (~610 ps) is assigned to the $S_1 \rightarrow T_1$ ISC time constant. ^{1}[**$Pyr_1RuPZn_2RuPyr_1$**]* → ^{3}[**$Pyr_1RuPZn_2RuPyr_1$**]* Φ_{ISC} can thus be calculated as ~56%. Considering that the fluorescence quantum yield of **$Pyr_1RuPZn_2RuPyr_1$** has been determined to be 2%, the ^{1}[**$Pyr_1RuPZn_2RuPyr_1$**]* → **$Pyr_1RuPZn_2RuPyr_1$** internal conversion ($S_1 \rightarrow S_0$) quantum yield (Φ_{IC}) is ~48%, whereas that determined for **$Pyr_1RuPZnRuPyr_1$** is ~0%. Such marked changes in Φ_{IC} for electronically excited **$Pyr_1RuPZn_2RuPyr_1$** relative to **$Pyr_1RuPZnRuPyr_1$** correlate with not only simple energy gap law predictions,[4] but also the data described above that determine significantly reduced $S_1 \rightarrow T_1$ ISC rate constants upon conjugation extension of **$Pyr_1RuPZnRuPyr_1$** to **$Pyr_1RuPZn_2RuPyr_1$** (**Table 3**).

B. $OsPZn_2Os$ and $Pyr_1RuPPt_2RuPyr_1$. With the same conjugated framework as **$Pyr_1RuPZn_2RuPyr_1$**, **$OsPZn_2Os$** and **$Pyr_1RuPPt_2RuPyr_1$** manifest substantially enhanced $S_1 \rightarrow T_1$ k_{ISC} and Φ_{ISC} values due to the stronger spin-orbit coupling effect induced by osmium or platinum. A common approach to modulate ISC dynamics takes advantage of the spin-orbit coupling effect. As the magnitude of spin-orbit coupling is roughly proportional to Z^4, where Z represents the nuclear charge,[5a,19] heavier metal nuclei that bind at either of the bis(terpyridyl)metal M or (porphinato)metal M' sites of the **M-(PM')$_n$-M** supermolecule can be exploited as tools to tune excited state relaxation dynamics and enhance excited-state singlet-triplet wavefunction mixing. As such, **$OsPZn_2Os$** and **$Pyr_1RuPPt_2RuPyr_1$** were synthesized to investigate the extent to which the nature of the bis(terpyridyl)metal and (porphinato)metal centers influence excited state relaxation dynamics.

Table 3. Dynamical Data [a], and Φ_{ISC} Values, Determined from Femtosecond-to-Nanosecond Transient Absorption Spectroscopic Experiments Examining **M-(PM')$_n$-M** Supermolecular Chromophores.

Chromophores	τ_{S1} [b] / ps	τ_F [c] / ps	τ_{ISC} [b] / ps	τ_T [d] / μs	Φ_{ISC} [e]
Pyr$_1$RuPZnRuPyr$_1$	0.8	N/A	0.77	9.0	~1
Pyr$_1$RuPZn$_2$RuPyr$_1$	340	305	610	9.9	0.56
OsPZn$_2$Os	31	26	28	0.4	~1
Pyr$_1$RuPPt$_2$RuPyr$_1$	0.28	N/A	0.39	2.9	~1
Pyr$_1$RuPZnPPtPZnRuPyr$_1$	36	30	34	4.4	~1
Pyr$_1$RuPZnPPdPZnRuPyr$_1$	155	150	190	13.0	0.82

[a] All data were acquired in acetonitrile solvent. [b] τ_{S1}, and τ_{ISC} values were determined using femtosecond transient absorption spectroscopic measurements. [c] Fluorescence lifetimes were determined via a Hamamatsu C4780 picosecond fluorescence lifetime measurement system. [d] τ_T values were determined using ns-to-μs time-domain transient absorption measurements. [e] Φ_{ISC} values were calculated based on dynamical data acquired using femtosecond transient absorption spectroscopy.

Compared to **Pyr$_1$RuPZn$_2$RuPyr$_1$**, **OsPZn$_2$Os** exhibits distinct excited state relaxation dynamics (**Figure 3a**). A global fit of the $S_1 \rightarrow S_n$ spectral region transient dynamical data reveals two relaxation processes: 1.8 ± 0.2 ps, 31 ± 4 ps. While the fast time constant (1.8 ps) is attributed to solvent relaxation dynamics, note that the 31 ps time constant agrees closely with the streakscope determined fluorescence lifetime (τ_F ~26 ps), and is therefore assigned as the intrinsic singlet lifetime of **OsPZn$_2$Os**. Given that the **OsPZn$_2$Os** intrinsic singlet lifetime timescale resembles the **PZn**-to-(terpyridyl)metal torsional dynamical timescale, [10c,20] **OsPZn$_2$Os** conformational dynamics may play a role in determining the S_1 state lifetime. The **OsPZn$_2$Os** S_1 state lifetime, an order magnitude smaller than that determined for **Pyr$_1$RuPZn$_2$RuPyr$_1$** (~340 ps), thus likely reflects faster ISC dynamics that correspondingly diminish its fluorescence quantum yield relative to **Pyr$_1$RuPZn$_2$RuPyr$_1$** (vide supra). Two characteristic relaxation times, 1.5 ± 0.2 ps and ~28 ± 3 ps, are obtained from global fitting of the $T_1 \rightarrow T_n$ transient spectral region, which correspond respectively to the solvent relaxation dynamics and the $S_1 \rightarrow T_1$ ISC time constant. The similarity between the S_1 state lifetime and τ_{ISC} in **OsPZn$_2$Os** emphasizes that the $S_1 \rightarrow T_1$ ISC is the dominant decay channel that depopulates the S_1 state, driving a near-unit Φ_{ISC}. Further transient absorption measurements carried out in the nanosecond-to-microsecond time domain determine an **OsPZn$_2$Os** T_1 state lifetime of ~0.4 μs (**Table 3**). Note that this T_1 state lifetime is dramatically reduced relative to that determined for **Pyr$_1$RuPZn$_2$RuPyr$_1$** (~9.9 μs), and congruent with osmium-enhanced spin-orbit coupling leading to enhanced $T_1 \rightarrow S_0$ ISC dynamics.

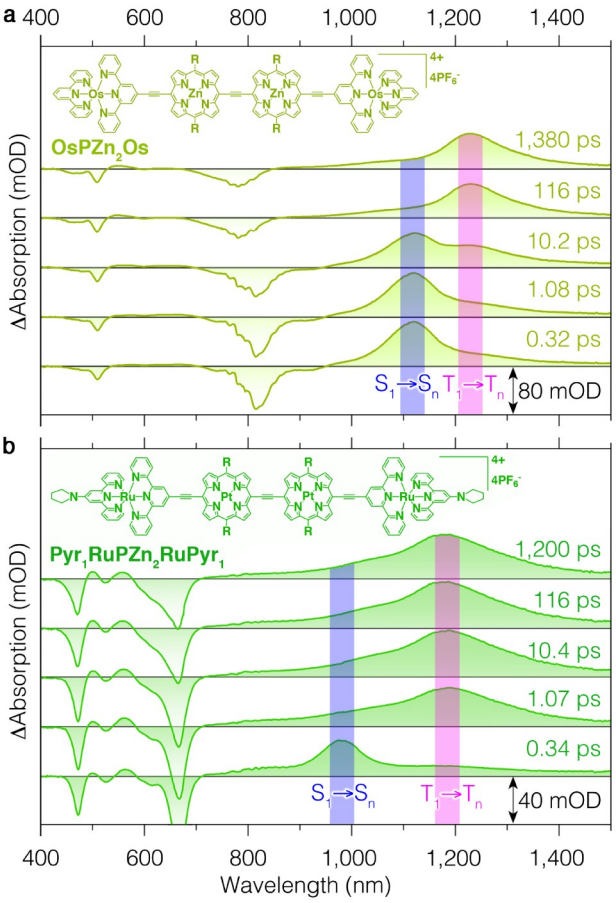

Figure 3. Transient absorption spectra determined at different time delays for (a) **OsPZn$_2$Os** (λ_{ex} = 820 nm), and (b) **Pyr$_1$RuPPt$_2$RuPyr$_1$** (λ_{ex} = 660 nm). Experimental conditions: ambient temperature, pump power = 300 μW, solvent = acetonitrile, magic angle polarization.

Representative transient representative spectra acquired for **Pyr$_1$RuPPt$_2$RuPyr$_1$** are shown in **Figure 3b**. In contrast to its analogue **Pyr$_1$RuPZn$_2$RuPyr$_1$**, which exhibits strong stimulated emission and an intense $S_1 \rightarrow S_n$ NIR transient absorption that remains prominent over the 0.3-120 ps time domain, **Pyr$_1$RuPPt$_2$RuPyr$_1$** transient spectra display no stimulated emission signal and a $S_1 \rightarrow S_n$ transient absorption that vanishes within 1 ps following optical excitation. Note, however, **Pyr$_1$RuPPt$_2$RuPyr$_1$** displays conformational dynamics and spectral diffusion in the Q-band bleach (**Figure S30**) similar to that manifested in **Pyr$_1$RuPZn$_2$RuPyr$_1$**. Global fitting of the $S_1 \rightarrow S_n$ spectral region transient dynamical data for **Pyr$_1$RuPPt$_2$RuPyr$_1$** reveals an ultrafast decay component of 280 ± 60 fs, whereas a corresponding analysis of the $T_1 \rightarrow T_n$ transient absorption data elucidates two dynamical processes: τ_1 = 390 ± 80 fs and τ_{Long}. The ultrafast time components evinced in the $S_1 \rightarrow S_n$ and $T_1 \rightarrow T_n$ transient absorptive spectral domains reflect the S_1 state lifetime and the ISC time constant, respectively, congruent with a near-unity Φ_{ISC}. Given the timescale of the acetonitrile solvent response, it is possible that solvent dynamics may be coupled to these ultrafast

excited state processes.[21] The long time constant associated with the $T_1 \rightarrow T_n$ transient kinetic data corresponds to excited triplet state relaxation; a T_1 lifetime of 2.91 ∝s was determined by nanosecond transient absorption measurements (**Figure S23**, and **Table 3**).

Despite the unit Φ_{ISC} of **OsPZn$_2$Os**, the diminished T_1-state lifetime (τ_T = 400 ns), however, makes this chromophore less useful in various optoelectronic applications, e.g. TTA-UC applications.[22] In the case of **Pyr$_1$RuPPt$_2$RuPyr$_1$**, the significant hypsochromic shift of the Q_x transition manifold ($\Delta\nu$ = 2361 cm^{-1}, *vide supra*) of this chromophore relative to the analogous family of transitions displayed by **Pyr$_1$RuPZn$_2$RuPyr$_1$**, make **Pyr$_1$RuPPt$_2$RuPyr$_1$** unsuitable for NIR photon capture, despite its ultrafast and unit quantum yield conversion to a long-lived T_1 state. With these considerations in mind, the following section highlights the versatility of **M-(PM')$_n$-M** chromophoric motif and demonstrates a molecular engineering approach that simultaneously delivers exceptional NIR absorptivity, ultrafast $S_1 \rightarrow T_1$ ISC dynamics, and long T_1–state lifetimes in these supermolecules.

C. Pyr$_1$RuPZnPPtPZnRuPyr$_1$ and Pyr$_1$RuPZnPPdPZnRuPyr$_1$. Representative transient absorption spectra acquired at selected time delays for **Pyr$_1$RuPZnPPtPZnRuPyr$_1$** and **Pyr$_1$RuPZnPPdPZnRuPyr$_1$** are shown in **Figure 4**; key spectral and dynamical data determined from these pump-probe transient absorption spectroscopic experiments are summarized in **Table 3**. As highlighted in **Figure 4**, **Pyr$_1$RuPZnPPtPZnRuPyr$_1$** and **Pyr$_1$RuPZnPPdPZnRuPyr$_1$** exhibit similar transient absorption features over the entire vis-NIR spectral domain interrogated in these experiments. For example, at early time delays (t < 10 ps), stimulated emission contributes significantly to the $S_1 \rightarrow S_n$ transition manifold bleaching signal centered near 800 nm. Global fitting of the NIR spectral region transient dynamical data acquired for **Pyr$_1$RuPZnPPtPZnRuPyr$_1$** and **Pyr$_1$RuPZnPPdPZnRuPyr$_1$** highlight noteworthy differences in the excited state relaxation dynamics important for these supermolecules. In the $S_1 \rightarrow S_n$ transition manifold region, **Pyr$_1$RuPZnPPtPZnRuPyr$_1$** manifests two time components: τ_1 = 950 ± 130 fs, τ_2 = 36 ± 4 ps. Given the time scale of τ_1, it is likely associated with solvent relaxation; the magnitude of τ_2 is close to the streak-scope determined fluorescence lifetime (τ_F = 30 ps), and therefore assigned as the intrinsic S_1 state lifetime (τ_{S1}) of **Pyr$_1$RuPZnPPtPZnRuPyr$_1$**. Near-identical characteristic time constants are obtained from fitting the $T_1 \rightarrow T_n$ transient absorption region of **Pyr$_1$RuPZnPPtPZnRuPyr$_1$**: τ_1 = 1.2 ± 0.2 ps, τ_2 = 34 ± 2 ps, consistent with τ_1 assignment as the solvent relaxation time, and τ_2 reflecting the ISC time constant. As τ_{S1} and τ_{ISC} are both ~35 ps, Φ_{ISC}(**Pyr$_1$RuPZnPPtPZnRuPyr$_1$**) ~1.

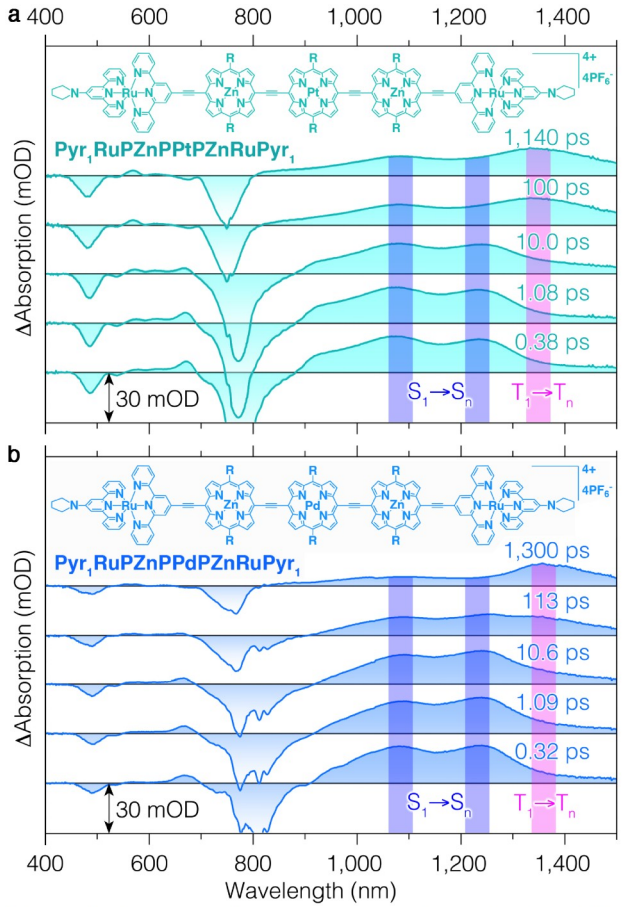

Figure 4. Transient absorption spectra determined at different time delays for (a) **Pyr $_1$RuPZnPPtPZnRuPyr $_1$** (λ_{ex} = 780 nm), and (b) **Pyr $_1$RuPZnPPdPZnRuPyr $_1$** (λ_{ex} = 800 nm). Experimental conditions: ambient temperature, pump power = 300 μW, solvent = acetonitrile, magic angle polarization.

An analogous global fit of the NIR spectral region transient dynamical data acquired for **Pyr$_1$RuPZnPPdPZnRuPyr$_1$** demonstrates three characteristic time components (τ_1 = 900 ± 60 fs, τ_2 = 42 ± 5 ps, τ_3 = 155 ± 9 ps) in the $S_1 \rightarrow S_n$ transition region, whereas fitting the $T_1 \rightarrow T_n$ spectral region reveals four time constants (τ_1 = 1.3 ± 0.2 ps, τ_2 = 39 ± 4 ps, τ_3 = 190 ± 8 ps, τ_{Long}). As discussed for related supermolecules detailed above, the magnitudes of τ_1 and τ_2 reflect respectively solvent and conformational relaxation dynamics. The 155 ps decay time agrees well with the measured fluorescence lifetime (150 ps), and is therefore attributed to the intrinsic S_1 state lifetime (τ_{S1}) of **Pyr$_1$RuPZnPPdPZnRuPyr$_1$**; consistent with the above analysis, the 190 ps time constant derived from fitting $T_1 \rightarrow T_n$ spectral region transient absorption data corresponds to the $S_1 \rightarrow T_1$ τ_{ISC}; thus, Φ_{ISC}(**Pyr$_1$RuPZnPPdPZnRuPyr$_1$**) is calculated to be ~82%.

5. State Energies and Design Principles for M-(PM')$_n$-M Supermolecular Chromophores. The nonradiative transition rate constant that characterizes the intersystem crossing process between the S_1 and T_1 states in

photoexcited chromophores can be expressed using a Fermi's Golden Rule formalism, in which the rate is proportional to the square of the spin-orbit coupling ($|\langle S_I|\hat{H}_{SO}|T_I\rangle|^2$) between the excited singlet and triplet states. [23] At a qualitative level, for these transition metal-containing supermolecules, it is important to note that the extent of molecular spin-orbit coupling depends on: i) the magnitude of the atomic coefficients of heavy metal d-orbitals that contribute to the one-electron excitation configurations describing the initially prepared singlet excited state wavefunction; and ii) the atomic spin-orbit coupling constants, ξ, of the heavy atoms in the supermolecular chromophore. [19,24] Quantitative determination of the extent to which one-electron excitations that feature appreciable metal d-orbital character contribute to the configuration expansions that describe the S_1 and T_1 wavefunctions of these electronically excited supermolecular chromophores is not computationally tractable; we describe, however, an alternative approach that qualitatively estimates the degree to which metal d orbital character contributes to the initially-prepared electronically excited singlet states in these **M-(PM')$_n$-M** chromophores.

In order to facilitate discussion of structure-property relationships important for engineering high Φ_{ISC}, long T_1 lifetimes (τ_{T1}), and high oscillator strength NIR absorptivity, Jablonski diagrams (**Figure 5**) have been constructed using ground-state electronic absorption, fluorescence, and phosphorescence data acquired for these **M-(PM')$_n$-M** chromophores. Note that a Jablonski diagram for the previously established asymmetric chromophore, **Pyr$_1$RuPZn**, has also been included in **Figure 5** for comparative purposes.

By comparing the excited-state relaxation dynamics among **Pyr$_1$RuPZn**, **Pyr$_1$RuPZnRuPyr$_1$**, and **Pyr$_1$RuPZn$_2$RuPyr$_1$**, we assess the influence of the conjugated framework on $|\langle S_1|\hat{H}_{SO}|T_1\rangle|^2$, the value of the spin–orbit coupling term upon the non-radiative $S_1 \rightarrow T_1$ transition in these **M-(PM')$_n$-M** structures. From a simple molecular-structure perspective, **Pyr$_1$RuPZn$_2$RuPyr$_1$** can be viewed as a construct built from connecting two identical **Pyr$_1$RuPZn** structures via an ethyne bridge. The fact that **Pyr$_1$RuPZn$_2$RuPyr$_1$** manifests a k_{ISC} value more than three orders of magnitude smaller (**Table 3**) than that determined for **Pyr$_1$RuPZn** underscores the disparate natures of their respective excited-state states. In contrast to **Pyr$_1$RuPZn** and **Pyr$_1$RuPZnRuPyr$_1$**, which manifest broad NIR transient absorptive manifolds characteristic of extensively delocalized T_1 states having substantial MLCT character at earliest time delays, and no evidence of stimulated emission in their respective transient absorption spectra, [14c,16] the time-dependent transient spectral evolution determined for **Pyr$_1$RuPZn$_2$RuPyr$_1$** (**Figure 2**) resembles that characteristic of the **PZn$_2$** chromophore (*vide supra*), [10c] underscoring that the $S_0 \rightarrow S_1$ transition of **Pyr$_1$RuPZn$_2$RuPyr$_1$** features augmented porphyrin-based π-π^* character relative to that characterizing the $S_0 \rightarrow S_1$

transitions of **Pyr$_1$RuPZn** and **Pyr$_1$RuPZnRuPyr$_1$**; this insight in turn indicates a reduced contribution of $[Ru(tpy)_2]^{2+}$-derived MLCT character to the initially prepared **Pyr$_1$RuPZn$_2$RuPyr$_1$** S_1 state wavefunction relative to these chromophores. Thus, the magnitude of the ruthenium d-orbital contributions to the one-electron excitation configurations describing the **Pyr$_1$RuPZn$_2$RuPyr$_1$** initially prepared singlet excited state is diminished relative to that for the analogous excited state for the **Pyr$_1$RuPZn** and **Pyr$_1$RuPZnRuPyr$_1$** chromophores, congruent with the dramatically reduced k_{ISC} and Φ_{ISC} observed for **Pyr$_1$RuPZn$_2$RuPyr$_1$**.

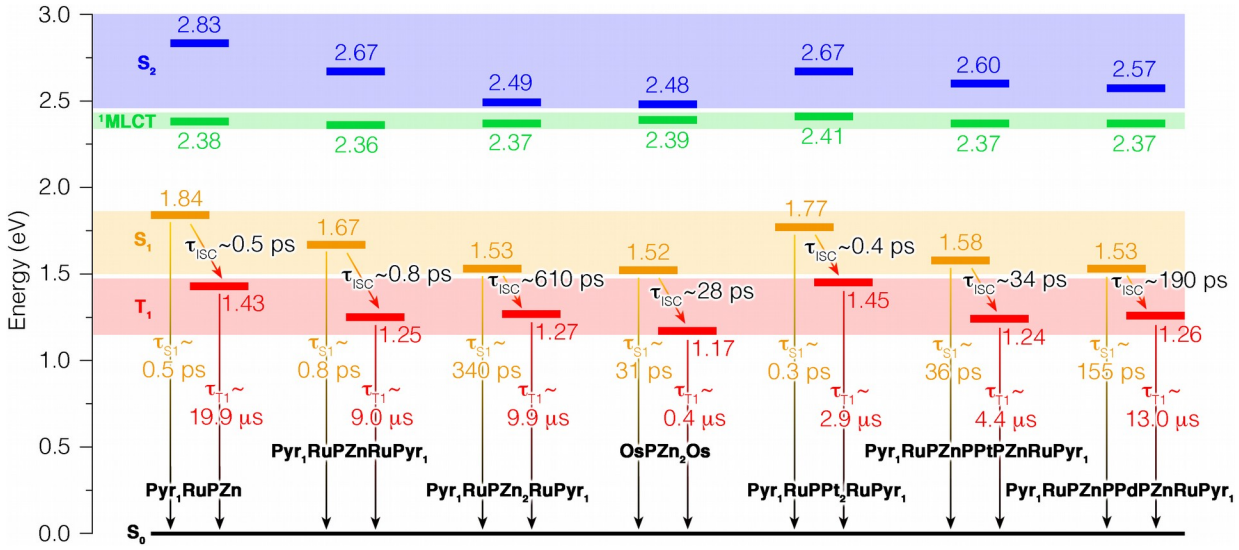

Figure 5. M-(PM')$_n$-M Jablonski diagrams highlighting the relative energetic separations of selected electronic states and relevant excited-state relaxation processes.

The impact of the (terpyridyl)metal heavy atom spin-orbit parameter (ξ_M) on the photophysics of these supermolecules are analyzed by comparing the Jablonski diagram of **OsPZn$_2$Os** with that of **Pyr$_1$RuPZn$_2$RuPyr$_1$** (**Figure 5**). While the **OsPZn$_2$Os** and **Pyr$_1$RuPZn$_2$RuPyr$_1$** NIR absorbers share an identical conjugated framework, the measured k_{ISC} for **OsPZn$_2$Os** ($k_{ISC} = 3.6\times10^{10}$ s^{-1}) is more than one order of magnitude larger than that measured for the **Pyr$_1$RuPZn$_2$RuPyr$_1$** supermolecule ($k_{ISC} = 1.6\times10^{9}$ s^{-1}). This increase of k_{ISC} must trace its genesis to the higher atomic spin orbit coupling constant of osmium(II) ion ($\xi_{Os} = 3000$ cm^{-1}) relative to ruthenium(II) ion ($\xi_{Ru} =$ 1000 cm^{-1}). These data suggest that the negative impact of conjugation expansion as chromophore structure evolves from **Pyr$_1$RuPZnRuPyr$_1$** to **Pyr$_1$RuPZn$_2$RuPyr$_1$** upon $|\langle S_1|\hat{H}_{SO}|T_1\rangle|^2$ may be compensated by exploiting (terpyridyl)metal units having larger atomic spin-orbit coupling constants (i.e., **OsPZn$_2$Os**). While **Pyr$_1$RuPZn$_2$RuPyr$_1$** and **OsPZn$_2$Os** have extraordinarily similar electronic absorption spectra (**Figure 3**), note that the osmium-enhanced spin-orbit coupling also drives corresponding enhanced $T_1 \rightarrow S_0$ ISC dynamics; **OsPZn$_2$Os** manifests a triplet excited state lifetime ($\tau_T = 0.4$ μs) more than twenty times shorter than that recorded for

Pyr$_1$RuPZn$_2$RuPyr$_1$ (τ_T = 9.9 μs). The combination of a lower-lying triplet excited state energy (T_1 = 1.16 eV, **Figure 5**) relative to **Pyr$_1$RuPZn$_2$RuPyr$_1$** (T_1 = 1.28 eV, **Figure 5**), and a diminished T_1 state lifetime, suggest that use of (terpyridyl)osmium centers in **M-(PM')$_n$-M** supermolecules do not constitute a viable approach to develop NIR absorbers with long-lived (~μs) triplet excited-state lifetimes that are required by many optoelectronic applications, such as TTA UC technologies where T_1-state energies are a critical consideration, and T_1 lifetimes of at least μs are required.[3a]

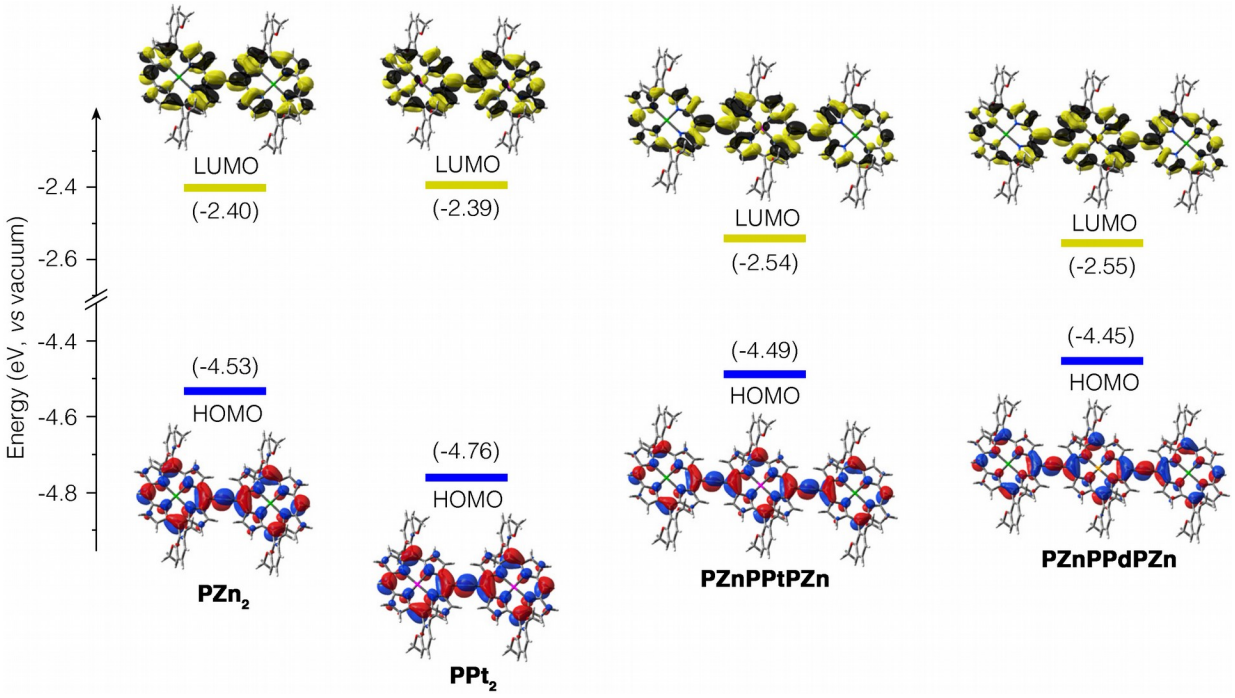

Figure 6. Frontier molecular orbitals (0.02 isodensity surfaces) for PZn_2, PPt_2, PZnPPtPZn, and PZnPPdPZn chromophores. Calculations were performed using B3LYP functional with 6-311g(d) basis set level, and minimal symmetry constraints; tight optimization criteria were applied in the geometry optimization processes.

The **Figure 5** Jablonski diagrams for **Pyr$_1$RuPZnRuPyr$_1$**, **OsPZn$_2$Os**, and **Pyr$_1$RuPZn$_2$RuPyr$_1$** suggest that further engineering of NIR chromophores with long-lived (μs) T_1 states produced at unit quantum yield should focus on manipulation of the electronic properties of the (porphinato)metal(II) building blocks of these supermolecules. Within this context, the Zn(II) metal ions of the parent **Pyr$_1$RuPZn$_2$RuPyr$_1$** chromophore were replaced by Pt (II) metal ions. The **Pyr$_1$RuPPt$_2$RuPyr$_1$** design relies on the facts that: (i) Platinum dπ orbitals interact more strongly with the porphyrin π-electron framework relative to the analogous zinc orbitals due to its larger atomic size.[25] As a result, the magnitude of the atomic coefficients of metal d-orbitals in **(PM')$_n$** fragment that contribute to the one-electron excitation configurations describing the initially prepared singlet excited state is increased in **Pyr$_1$RuPPt$_2$RuPyr$_1$** relative to the case in **Pyr$_1$RuPZn$_2$RuPyr$_1$**. (ii) The atomic spin-orbit coupling constant of

platinum (ξ_{Pt} = 4441 cm^{-1}) is an order of magnitude stronger than that of zinc (ξ_{Zn} = 390 cm^{-1}).[26] Congruent with this design, population analysis of the frontier orbital (FO) electron densities shows non-modest Pt d-orbital contributions (Supporting Information, Section 7) to orbitals important to the one-electron transitions that figure prominently in the configuration expansions that describe the low-lying excited states of the **Pyr $_1$RuPPt$_2$RuPyr$_1$** supermolecule; for example, the Pt-d orbital contributes 2.9 % of the **PPt $_2$** LUMO electron density (**Table S1; Figure 6**), contrasting the case for **PZn$_2$**, where Zn-d orbital electron density contributes just 0.3 % to the LUMO (**Figure S32**). Congruent with the combination of these effects, k_{ISC} for **Pyr$_1$RuPPt$_2$RuPyr$_1$** increases by three orders of magnitude relative to that measured for **Pyr $_1$RuPZn$_2$RuPyr$_1$** (**Figure 5**), and Φ_{ISC} for **Pyr$_1$RuPPt$_2$RuPyr$_1$** is driven to unity. While the large magnitude manifold hypsochromic shift of the ^{1}Qx-derived transition manifold of **Pyr $_1$RuPPt$_2$RuPyr$_1$** (λ_{1Qx}(max) = 653 nm) relative to **Pyr $_1$RuPZn$_2$RuPyr$_1$ (**λ_{1Qx}(max) = 772 nm) makes the **Pyr $_1$RuPPt$_2$RuPyr$_1$** supermolecule unsuitable for harvesting NIR photons (**Figure 3**), this composition provides important chromophore design insights: as **Pyr $_1$RuPPt$_2$RuPyr$_1$** manifests a substantial triplet excited state lifetime (τ_T = 2.9 μs), it indicates heavy atom substitution of the **(PM') $_n$** chromophoric fragment of **M-(PM') $_n$-M** supermolecules provides a feasible path to augment S_1-T_1 ISC rate constants that will not necessarily drive $T_1 \rightarrow S_0$ relaxation dynamics into the sub-μs time regime.

To achieve near-unit Φ_{ISC} while maintaining high oscillator strength NIR absorptivity within **M-(PM') $_n$-M** supermolecules, we designed **Pyr $_1$RuPZnPM'PZnRuPyr $_1$** (**M'** = **Pt**, **Pd**) hybrid chromophores based on *meso*-to-*meso* ethyne-bridged (porphinato)metal(II) trimers in which only the central porphyrin unit is complexed with Pd(II) or Pt(II) heavy metals ions (**Scheme 1**). TD-DFT calculations performed on **PZnPM'PZn (M = Pd**, **Pt)** model chromophores determine that the HOMO→LUMO one-electron transition figures prominently in the configuration expansions that describe the globally delocalized S_1 excited states of these supermolecules (**Figure S32**); population analysis of the FO electron densities shows that the Pt-d orbitals contribute 1.3 % of the overall electron density of the **PZnPPtPZn** LUMO (**Table S3; Figure 6**), while the analogous Pd d-orbitals account for 0.7 % (**Table S4**) of **PZnPPdPZn** LUMO electron density. Due to larger magnitude of the atomic coefficients (1.3 %) of Pt-d orbitals that contribute to the FOs of **PZnPPtPZn** relative to that (0.7 %) of the Pd-d orbitals contributing to the FOs of **PZnPPdPZn**, and the significantly larger spin-orbit coupling constant of Pt (ξ_{Pt} = 4481 cm^{-1}) than that of Pd (ξ_{pd} = 1500 cm^{-1}), **Pyr$_1$RuPZnPPtPZnRuPyr $_1$** displays larger magnitude k_{ISC} (3.0×10^{10} s^{-1}) and Φ_{ISC} (~ 1) values relative to **Pyr$_1$RuPZnPPdPZnRuPyr $_1$** (k_{ISC} ~5.3×10^{9} s^{-1}, Φ_{ISC} ~0.82). We note that both of these supermolecular

chromophores possess substantial triplet state lifetimes [(τ_{T1} (**Pyr$_1$RuPZnPPtPZnRuPyr$_1$**) = 4.4 μs; τ_{T1} (**Pyr$_1$RuPZnPPdPZnRuPyr$_1$**) = 13.0 μs). These data underscore that divalent Pt and Pd ions within the **(PM')$_n$** chromophoric fragment of **M-(PM')$_n$-M** supermolecules can be exploited as tools to tune the magnitude of the atomic coefficients of heavy metal d-orbitals that contribute to the one-electron excitation configurations describing the initially prepared singlet excited state: introduction of a single **PPt** or **PPd** unit within **the (PM')$_n$** fragment of **M-(PM')$_n$-M** supermolecules makes possible both high oscillator strength NIR absorptivity and substantial ISC quantum yield, without detrimental impact upon $T_1 \rightarrow S_0$ relaxation dynamics. This ability to simultaneously fine tune the relative magnitudes of k^0_F, k_{nr}, k_{ISC}, and $k_{T1 \rightarrow S0}$ is currently unrivaled in other chromophoric platforms, and highlights the utility of this molecular roadmap to design NIR absorbers having highly modulated photophysical properties. **Figure 7** summarizes the overall molecular design approach to realize exceptional NIR absorbers that possess long-lived triplet excited-states produced at near-unit Φ_{ISC} through modulation of the **M-(PM')$_n$-M** supermolecular platform.

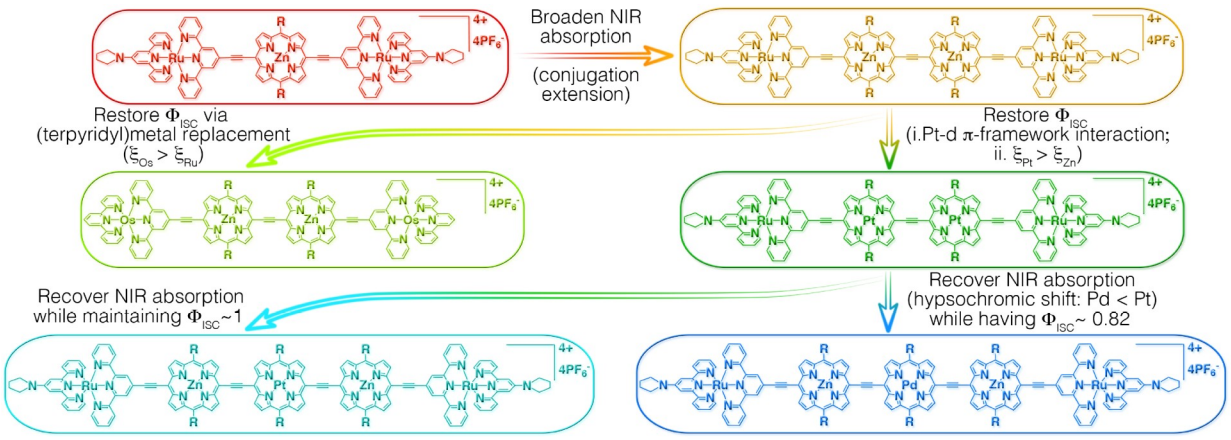

Figure 7. Molecular design flow for realizing exceptional NIR absorbers that possess long-lived triplet excited-states produced at near-unit Φ_{ISC} through modulation of the **M-(PM')$_n$-M** supermolecular platform.

With respect to **Figures 5** and **7**, it is important to consider that radiationless transition theory expresses the ISC rate constant in terms of (i) a state density factor, (ii) a matrix element describing the spin-orbit coupling between the S_1 and T_1 wave functions ($|\langle S_1|\hat{H}_{SO}|T_1\rangle|^2$), and (iii) an overlap factor that accounts for the diminution of the nonradiative rate constant magnitudes with increasing $\Delta E_{S1\text{-}T1}$.[23a,27] In many families of transition metal chromophores, the magnitude of k_{ISC} tracks smoothly with $(\Delta E_{S1\text{-}T1})^{-1}$. Such a dependence is clearly not manifest in the photophysics of these **M-(PM')$_n$-M** supermolecules (**Figure 5**), underscoring the importance of manipulating the

extent to which heavy metal d-orbitals contribute to the one-electron excitation configurations that describe the initially prepared singlet excited states of these chromophores (*vide supra*).

We point out that while the optical band gap can be extensively modulated within this family of **M-(PM')$_n$-M** supermolecules, **Pyr$_1$RuPZnRuPyr$_1$**, **Pyr$_1$RuPZn$_2$RuPyr$_1$**, **Pyr$_1$RuPZnPPtPZnRuPyr$_1$**, and **Pyr$_1$RuPZnPPdPZnRuPyr$_1$** possess extraordinarily similar S_0-T_1 energy gaps (**Figure 5**). Such an observation is congruent with the notion that the spatial extent of the T_1-wavefunctions of **M-(PM')$_n$-M** supermolecules are more localized than their corresponding low-lying singlet excited states. This supposition is congruent with the previous EPR spectroscopic investigations of the electronically excited triplet states ethyne-bridged multi-porphyrin compounds.[10d,10g,28] Given the highly uniform S_0-T_1 energy gaps for these supermolecules, the magnitude of $\Delta E_{S1\text{-}T1}$ ranges from 0.42 eV (**Pyr$_1$RuPZnRuPyr$_1$**) to 0.27 eV (**Pyr$_1$RuPZnPPdPZnRuPyr$_1$**). In this regard, we note that the Pd- derived supermolecule, **Pyr$_1$RuPZnPPdPZnRuPyr$_1$**, manifests relative S_1-T_1 energy levels that stand in sharp contrast to those of classic porphyrinic chromophores, (polypyridyl)ruthenium(II) / osmium(II) complexes, and other π-conjugated polymers that are characterized by large Φ_{ISC} values, as these chromophores evince $\Delta E_{S1\text{-}T1}$ gaps that exceed 0.4 eV.[11,18,29]

With respect to the potential utility of these **M-(PM')$_n$-M** supermolecules in OPL applications, we note that OPL schemes based on reverse saturable absorption typically requires materials having weak ground-state ($S_0 \rightarrow S_1$) absorption, but substantial $T_1 \rightarrow T_n$ absorptive oscillator strength in the operational wavelength regime.[1,30] Furthermore, the ISC time constant of such OPL materials should be shorter than the laser pulse duration.[30] In these respects, we note that **M-(PM')$_n$-M** display weak but non-negligible absorption up to ~1000 nm (*e.g.*, $\varepsilon_{\lambda = 800\ nm}$ ($S_0 \rightarrow S_1$, **Pyr$_1$RuPPt$_2$RuPyr$_1$**) ~360 M^{-1} cm^{-1}, $\varepsilon_{\lambda = 950\ nm}$ ($S_0 \rightarrow S_1$, **Pyr$_1$RuPZnPPtPZnRuPyr$_1$**) ~800 M^{-1} cm^{-1}, $\varepsilon_{\lambda = 1000\ nm}$ ($S_0 \rightarrow S_1$, **Pyr$_1$RuPZnPPdPZnRuPyr$_1$**) ~600 M^{-1} cm^{-1}), but corresponding $T_1 \rightarrow T_n$ excited-state absorption extinction coefficients that are enormous ($\varepsilon_{\lambda = 1000\ nm}$ ($T_1 \rightarrow T_n$, **Pyr$_1$RuPPt$_2$RuPyr$_1$**) ~ 7000 M^{-1} cm^{-1}, $\varepsilon_{\lambda = 1000\ nm}$ ($T_1 \rightarrow T_n$, **Pyr$_1$RuPZnPPtPZnRuPyr$_1$**) ~40000 M^{-1} cm^{-1}, $\varepsilon_{\lambda = 1000\ nm}$ ($T_1 \rightarrow T_n$, **Pyr$_1$RuPZnPPdPZnRuPyr$_1$**) ~48000 M^{-1} cm^{-1}; procedures for estimating $\varepsilon_{T1 \rightarrow Tn}$ have been detailed elsewhere [14c]). Moreover, as the ISC time constants for these compounds ranges from ~0.4 to ~190 ps, these and related chromophores should be well poised for NIR OPL in which sub-ps to sub-ns laser pulses are exploited; the potential utility of these structures is further underscored by the paucity of high performance optical limiting materials that function near1000 nm.

For NIR TTA UC, a critical hurdle to real-world applications of this technology includes the lack of

appropriate NIR-absorbing sensitizers that simultaneously feature: (i) broad, high oscillator strength spectral absorptivity beyond 700 nm, (ii) near-unit singlet-to-triplet intersystem crossing quantum (ISC) yields that do not occur with significant loss of excited-state energy, (iii) T_1 states having a sufficiently long (≥ μs) lifetimes, and (iv) T_1 state energy levels that assure exergonic triplet-triplet energy transfer to the annihilator. [3] In this regard, **Pyr$_1$RuPZnPM'PZnRuPyr$_1$** chromophores are well suited for NIR TTA UC, as they not only meet the excited-state dynamical requirements, but also display exceptional ground-state absorptivity beyond 750 nm and T_1 state energy levels appropriate for sensitizing commonly used annihilators, (*e.g.* rubrene [3a]).

Conclusion

A molecular design roadmap has been described that realizes chromophores that simultaneously possess substantial near-infrared (NIR) absorptivity and long-lived, high-yield triplet excited states. These designs circumvent the critical energy-gap-law hurdle whereby diminishing absorber optical bandgap exponentially increases nonradiative ($S_1 \rightarrow S_0$) transition rate constants and reduces $S_1 \rightarrow T_1$ intersystem crossing (ISC) quantum yields. This chromophore design methodology exploits the ethyne-bridged (polypyridyl)metal(II) (**M**; **M** = **Ru**, **Os**)-(porphinato)metal(II) (**PM'**; **M'** = **Zn**, **Pt**, **Pd**) molecular architecture (**M-(PM')$_n$-M**), where the nature of the supermolecular conjugation drives substantial mixing of porphyrin-based π-π* and metal polypyridyl-based charge-resonance transitions. By varying the extent to which the atomic coefficients of heavy metal d-orbitals contribute to the one-electron excitation configurations describing the initially prepared singlet and triplet excited-state wavefunctions, the relative magnitudes of fluorescence (k_F^0), $S_1 \rightarrow S_0$ non-radiative decay (k_{nr}), $S_1 \rightarrow T_1$ ISC (k_{ISC}), and $T_1 \rightarrow S_0$ relaxation ($k_{T1 \rightarrow S0}$) rate constants can be finely tuned in **M-(PM')$_n$-M** compounds; such insights in turn enable molecular designs in which the k_{ISC} magnitude dominates singlet manifold relaxation dynamics, but does not give rise to $T_1 \rightarrow S_0$ conversion dynamics that short-circuit a μs timescale triplet lifetime.

The **M-(PM')$_n$-M** supermolecular chromophore structure-function relationships derived from these studies are reflected, for example, in the designs of **Pyr$_1$RuPZnPM'PZnRuPyr$_1$** (**M'** = **Pt**, **Pd**) chromophores: **Pyr$_1$RuPPZnPdPZnRuPyr$_1$** ($\varepsilon_{780\,nm} = 1.63 \times 10^5\ M^{-1}cm^{-1}$, f_{NIR} ~1.13, Φ_{ISC} ~82%, τ_{T1} ~13.0 μs, $\Delta E_{S1\text{-}T1} = 0.27$ eV); **Pyr$_1$RuPPZnPtPZnRuPyr$_1$** ($\varepsilon_{750\,nm} = 1.50 \times 10^5\ M^{-1}cm^{-1}$, f_{NIR} ~0.85, Φ_{ISC} ~100%, τ_{T1} ~4.4 μs, $\Delta E_{S1\text{-}T1} = 0.34$ eV). Given these enhanced NIR-absorptive and photophysical properties, **M-(PM')$_n$-M** chromophores stand in sharp contrast to extensive families of conventional metal complexes, organic molecules, and polymer materials such as

(polypyridyl)metal(II) complexes, [11] bodipy derivatives, [3b] and polythiophene derivatives [12] that have been traditionally exploited as long-wavelength absorbers that give rise to substantial electronically excited triplet state populations. Chromophores derived from **M-(PM')$_n$-M** supermolecular architectures open new opportunities to construct exceptional NIR-absorbers that not only possess long-lived triplet excited states produced at high quantum yield: as both absolute T_1 state energies may be controlled while ensuring modest S_1-T_1 state energy gaps, such chromophores are uniquely poised to impact optical power limiting, dye-sensitized solar cell, and photon-upconversion applications.

ASSOCIATED CONTENT

Supporting Information Available: Synthetic details and characterization data for all the ethyne-bridged (polypyridyl)metal(II)-(porphinato)metal(II) species and their corresponding precursor compounds, detailed review regarding the steady-state and time-resolved emission, nanosecond transient absorption, dynamics and global analysis, TD-DFT calculated transitions and computational details for oligo(porphinato)metal(II) molecular structures. This material is available free of charge via the Internet at http://pubs.acs.org.

AUTHOR INFORMATION

Corresponding Author: *michael.therien@duke.edu

Notes: The authors declare no competing financial interest.

ACKNOWLEDGMENT

The authors acknowledge the National Science Foundation for support of this work through grant CHE-1709497. Early stages of this research were supported through a grant from the DOE-EERE Sunshot Program (XEV-2-22202). Y.B. gratefully acknowledges the generous support from the Fitzpatrick Institute of Photonics at Duke University for a John T. Chambers Scholars Award.

References:

(1) Spangler, C. W. *J. Mater. Chem.* **1999**, *9*, 2013-2020.
(2) (a) Hagfeldt, A.; Boschloo, G.; Sun, L. C.; Kloo, L.; Pettersson, H. *Chem. Rev.* **2010**, *110*, 6595-6663. (b) Grätzel, M. *J. Photochem. Photobiol. C: Photochem. Rev.* **2003**, *4*, 145-153.
(3) (a) Singh-Rachford, T. N.; Castellano, F. N. *Coord. Chem. Rev.* **2010**, *254*, 2560-2573. (b) Zhao, J. Z.; Wu, W. H.; Sun, J. F.; Guo, S. *Chem. Soc. Rev.* **2013**, *42*, 5323-5351. (c) Zhao, J. Z.; Ji, S. M.; Guo, H. M. *Rsc Adv.* **2011**, *1*, 937-950.
(4) Englman, R.; Jortner, J. *Mol. Phys.* **1970**, *18*, 145-164.
(5) (a) Turro, N. J.; Ramamurthy, V.; Scaiano, J. C. *Modern molecular photochemistry of organic molecules*; University Science Books: Sausalito, CA, 2010. (b) Bixon, M.; Jortner, J. *J. Chem. Phys.* **1968**, *48*, 715-726. (c)

Caspar, J. V.; Meyer, T. J. *J. Phys. Chem.* **1983**, *87*, 952-957. (d) Wilson, J. S.; Chawdhury, N.; Al-Mandhary, M. R. A.; Younus, M.; Khan, M. S.; Raithby, P. R.; Kohler, A.; Friend, R. H. *J. Am. Chem. Soc.* **2001**, *123*, 9412-9417.
(6) (a) Balzani, V.; Juris, A.; Venturi, M.; Campagna, S.; Serroni, S. *Chem. Rev.* **1996**, *96*, 759-833. (b) Islangulov, R. R.; Castellano, F. N. *Angew. Chem. Int. Ed.* **2006**, *45*, 5957-5959. (c) Ardo, S.; Meyer, G. J. *Chem. Soc. Rev.* **2009**, *38*, 115-164. (d) Youngblood, W. J.; Lee, S. H. A.; Maeda, K.; Mallouk, T. E. *Acc. Chem. Res.* **2009**, *42*, 1966-1973.
(7) (a) Hirth, A.; Vollrath, K.; Faure, J.; Lougnot, D. *Opt. Commun.* **1973**, *7*, 339-342. (b) Decker, C. D. *Appl. Phys. Lett.* **1975**, *27*, 607-609. (c) Romanek, K. M.; Hildebrand, O.; Göbel, E. *Opt. Commun.* **1977**, *21*, 16-19. (d) Kranitzky, W.; Kopainsky, B.; Kaiser, W.; Drexhage, K. H.; Reynolds, G. A. *Opt. Commun.* **1981**, *36*, 149-152. (e) Arthurs, E. G.; Bradley, D. J.; Roddie, A. G. *Appl. Phys. Lett.* **1972**, *20*, 125-127.
(8) (a) Mathew, S.; Yella, A.; Gao, P.; Humphry-Baker, R.; Curchod, B. F. E.; Ashari-Astani, N.; Tavernelli, I.; Rothlisberger, U.; Nazeeruddin, M. K.; Grätzel, M. *Nat. Chem.* **2014**, *6*, 242-247. (b) Li, L. L.; Diau, E. W. G. *Chem. Soc. Rev.* **2013**, *42*, 291-304. (c) Campbell, W. M.; Burrell, A. K.; Officer, D. L.; Jolley, K. W. *Coord. Chem. Rev.* **2004**, *248*, 1363-1379. (d) Rawson, J.; Stuart, A. C.; You, W.; Therien, M. J. *J. Am. Chem. Soc.* **2014**, *136*, 17561-17569.
(9) (a) Lin, V. S.-Y.; DiMagno, S. G.; Therien, M. J. *Science* **1994**, *264*, 1105-1111. (b) Lin, V. S.-Y.; Therien, M. J. *Chem. Eur. J.* **1995**, *1*, 645-651. (c) Anderson, H. L. *Inorg. Chem.* **1994**, *33*, 972-981. (d) Tsuda, A.; Osuka, A. *Science* **2001**, *293*, 79-82. (e) Aratani, N.; Osuka, A.; Kim, Y. H.; Jeong, D. H.; Kim, D. *Angew. Chem. Int. Ed.* **2000**, *39*, 1458-1462. (f) Taniguchi, M.; Cramer, D. L.; Bhise, A. D.; Kee, H. L.; Bocian, D. F.; Holten, D.; Lindsey, J. S. *New J. Chem.* **2008**, *32*, 947-958. (g) Alexy, E. J.; Yuen, J. M.; Chandrashaker, V.; Diers, J. R.; Kirmaier, C.; Bocian, D. F.; Holten, D.; Lindsey, J. S. *Chem. Commun.* **2014**, *50*, 14512-14515. (h) Vairaprakash, P.; Yang, E.; Sahin, T.; Taniguchi, M.; Krayer, M.; Diers, J. R.; Wang, A.; Niedzwiedzki, D. M.; Kirmaier, C.; Lindsey, J. S.; Bocian, D. F.; Holten, D. *J. Phys. Chem. B* **2015**, *119*, 4382-4395.
(10) (a) Roberts, D. A.; Fuckel, B.; Clady, R. G. C. R.; Cheng, Y. Y.; Crossley, M. J.; Schmidt, T. W. *J. Phys. Chem. A* **2012**, *116*, 7898-7905. (b) Cho, H. S.; Jeong, D. H.; Cho, S.; Kim, D.; Matsuzaki, Y.; Tanaka, K.; Tsuda, A.; Osuka, A. *J. Am. Chem. Soc.* **2002**, *124*, 14642-14654. (c) Rubtsov, I. V.; Susumu, K.; Rubtsov, G. I.; Therien, M. J. *J. Am. Chem. Soc.* **2003**, *125*, 2687-2696. (d) Shediac, R.; Gray, M. H. B.; Uyeda, H. T.; Johnson, R. C.; Hupp, J. T.; Angiolillo, P. J.; Therien, M. J. *J. Am. Chem. Soc.* **2000**, *122*, 7017-7033. (e) Chang, M. H.; Hoffmann, M.; Anderson, H. L.; Herz, L. M. *J. Am. Chem. Soc.* **2008**, *130*, 10171-10178. (f) Winters, M. U.; Karnbratt, J.; Eng, M.; Wilson, C. J.; Anderson, H. L.; Albinsson, B. *J. Phys. Chem. C* **2007**, *111*, 7192-7199. (g) Angiolillo, P. J.; Lin, V. S.-Y.; Vanderkooi, J. M.; Therien, M. J. *J. Am. Chem. Soc.* **1995**, *117*, 12514-12527. (h) Duncan, T. V.; Susumu, K.; Sinks, L. E.; Therien, M. J. *J. Am. Chem. Soc.* **2006**, *128*, 9000-9001. (i) Wang, J. Q.; Yang, E.; Diers, J. R.; Niedzwiedzki, D. M.; Kirmaier, C.; Bocian, D. F.; Lindsey, J. S.; Holten, D. *J. Phys. Chem. B* **2013**, *117*, 9288-9304.
(11) Sauvage, J. P.; Collin, J. P.; Chambron, J. C.; Guillerez, S.; Coudret, C.; Balzani, V.; Barigelletti, F.; Decola, L.; Flamigni, L. *Chem. Rev.* **1994**, *94*, 993-1019.
(12) (a) Kraabel, B.; Moses, D.; Heeger, A. J. *J. Chem. Phys.* **1995**, *103*, 5102-5108. (b) Guo, J. M.; Ohkita, H.; Benten, H.; Ito, S. *J. Am. Chem. Soc.* **2009**, *131*, 16869-16880. (c) Sugimoto, T.; Ebihara, Y.; Ogino, K.; Vacha, M. *ChemPhysChem* **2007**, *8*, 1623-1628.
(13) Park, J.; Deria, P.; Therien, M. J. *J. Am. Chem. Soc.* **2011**, *133*, 17156-17159.
(14) (a) Susumu, K.; Therien, M. J. *J. Am. Chem. Soc.* **2002**, *124*, 8550-8552. (b) Uyeda, H. T.; Zhao, Y. X.; Wostyn, K.; Asselberghs, I.; Clays, K.; Persoons, A.; Therien, M. J. *J. Am. Chem. Soc.* **2002**, *124*, 13806-13813. (c) Duncan, T. V.; Ishizuka, T.; Therien, M. J. *J. Am. Chem. Soc.* **2007**, *129*, 9691-9703.
(15) (a) Takahashi, S.; Kuroyama, Y.; Sonogashira, K.; Hagihara, N. *Synth.* **1980**, 627-630. (b) DiMagno, S. G.; Lin, V. S.-Y.; Therien, M. J. *J. Org. Chem.* **1993**, *58*, 5983-5993. (c) DiMagno, S. G.; Lin, V. S.-Y.; Therien, M. J. *J. Am. Chem. Soc.* **1993**, *115*, 2513-2515. (d) LeCours, S. M.; Guan, H. W.; DiMagno, S. G.; Wang, C. H.; Therien, M. J. *J. Am. Chem. Soc.* **1996**, *118*, 1497-1503.
(16) Duncan, T. V.; Rubtsov, I. V.; Uyeda, H. T.; Therien, M. J. *J. Am. Chem. Soc.* **2004**, *126*, 9474-9475.
(17) (a) Eastwood, D.; Gouterman, M. *J. Mol. Spectrosc.* **1970**, *35*, 359-375. (b) Gouterman, M. *Optical Spectra and Electronic Structure of Porphyrin*; Academic Press: New York, 1978. (c) Harriman, A. *J. Chem. Soc. Faraday Trans. 2* **1981**, *77*, 1281-1291.
(18) Duncan, T. V.; Frail, P. R.; Miloradovic, I. R.; Therien, M. J. *J. Phys. Chem. B* **2010**, *114*, 14696-14702.
(19) Khudyakov, I. V.; Serebrennikov, Y. A.; Turro, N. J. *Chem. Rev.* **1993**, *93*, 537-570.
(20) Kumble, R.; Palese, S.; Lin, V. S.-Y.; Therien, M. J.; Hochstrasser, R. M. *J. Am. Chem. Soc.* **1998**, *120*, 11489-11498.
(21) McCusker, J. K. *Acc. Chem. Res.* **2003**, *36*, 876-887.

(22) Olivier, J. H.; Bai, Y. S.; Uh, H.; Yoo, H.; Therien, M. J.; Castellano, F. N. *J. Phys. Chem. A* **2015**, *119*, 5642-5649.
(23) (a) Marian, C. M. *WIREs Comput. Mol. Sci.* **2012**, *2*, 187-203. (b) Sousa, C.; de Graaf, C.; Rudavskyi, A.; Broer, R.; Tatchen, J.; Etinski, M.; Marian, C. M. *Chem. Eur. J.* **2013**, *19*, 17541-17551.
(24) Cannizzo, A.; Blanco-Rodriguez, A. M.; El Nahhas, A.; Sebera, J.; Zalis, S.; Vlcek, A.; Chergui, M. *J. Am. Chem. Soc.* **2008**, *130*, 8967-8974.
(25) (a) Armaroli, N.; Diederich, F.; Echegoyen, L.; Habicher, T.; Flamigni, L.; Marconi, G.; Nierengarten, J. F. *New J. Chem.* **1999**, *23*, 77-83. (b) Mink, L. M.; Neitzel, M. L.; Bellomy, L. M.; Falvo, R. E.; Boggess, R. K.; Trainum, B. T.; Yeaman, P. *Polyhedron* **1997**, *16*, 2809-2817. (c) Tokel-Takvoryan, N. E.; Bard, A. J. *Chem. Phys. Lett.* **1974**, *25*, 235-238.
(26) Montalti, M.; Murov, S. L. *Handbook of Photochemistry*; 3rd ed.; CRC/Taylor & Francis: Boca Raton, FL, 2006.
(27) Beljonne, D.; Cornil, J.; Friend, R. H.; Janssen, R. A. J.; Bredas, J. L. *J. Am. Chem. Soc.* **1996**, *118*, 6453-6461.
(28) (a) Angiolillo, P. J.; Susumu, K.; Uyeda, H. T.; Lin, V. S.-Y.; Shediac, R.; Therien, M. J. *Synth. Met.* **2001**, *116*, 247-253. (b) Angiolillo, P. J.; Uyeda, H. T.; Duncan, T. V.; Therien, M. J. *J. Phys. Chem. B* **2004**, *108*, 11893-11903. (c) Richert, S.; Bullard, G.; Rawson, J.; Angiolillo, P. J.; Therien, M. J.; Timmel, C. R. *J. Am. Chem. Soc.* **2017**, *139*, 5301-5304.
(29) Monkman, A. P.; Burrows, H. D.; Hartwell, L. J.; Horsburgh, L. E.; Hamblett, I.; Navaratnam, S. *Phys. Rev. Lett.* **2001**, *86*, 1358-1361.
(30) Zhou, G. J.; Wong, W. Y. *Chem. Soc. Rev.* **2011**, *40*, 2541-2566.

TOC:

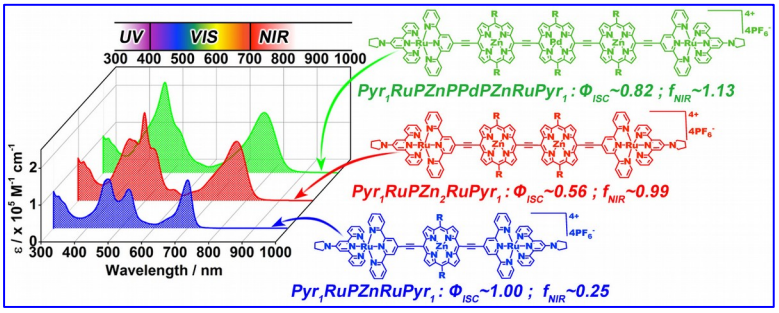
UV
VIS
NIR
300 400 500 600 700 800 900 1000
ε / x 10^5 M^-1 cm^-1
2
1
0
300 400 500 600 700 800 900 1000
Wavelength / nm
Pyr1RuPZnPPdPZnRuPyr1 : ΦISC~0.82 ; fNIR~1.13
Pyr1RuPZn2RuPyr1 : ΦISC~0.56 ; fNIR~0.99
Pyr1RuPZnRuPyr1 : ΦISC~1.00 ; fNIR~0.25